Key Points:
- Most confined aquifers may be leaking to some extent; here we derive a new model for the tidal response of a leaky aquifer
- Leakage may be estimated from Earth tide analysis if the transmissivity and storativity of the aquifer are known independently
- Applying the model to interpret the water level tides in an Oklahoma deep well shows that the Arbuckle aquifer may be leaking significantly

Tidal Response of Groundwater in a Leaky Aquifer—Application to Oklahoma

Chi-Yuen Wang[1] [ID]**, Mai-Linh Doan[2]** [ID]**, Lian Xue[1], and Andrew J. Barbour[3]** [ID]

[1]Department of Earth and Planetary Science, University of California, Berkeley, CA, USA, [2]University Grenoble Alpes, University Savoie Mont Blanc, CNRS, IRD, IFSTTAR, ISTerre, Grenoble, France, [3]Earthquake Science Center, U.S. Geological Survey, Menlo Park, CA, USA

Abstract Quantitative interpretation of the tidal response of water levels measured in wells has long been made either with a model for perfectly confined aquifers or with a model for purely unconfined aquifers. However, many aquifers may be neither totally confined nor purely unconfined at the frequencies of tidal loading but behave somewhere between the two end-members. Here we present a more general model for the tidal response of groundwater in aquifers with both horizontal flow and vertical leakage. The model has three independent parameters: the transmissivity (T) and storativity (S) of the aquifer and the specific leakage (K'/b') of the leaking aquitard, where K' and b' are the hydraulic conductivity and the thickness of the aquitard, respectively. If T and S are known independently, this model may be used to estimate aquitard leakage from the phase shift and amplitude ratio of water level in wells obtained from tidal analysis. We apply the model to interpret the tidal response of water level in a US Geological Survey (USGS) deep monitoring well installed in the Arbuckle aquifer in Oklahoma, into which massive amount of wastewater coproduced from hydrocarbon exploration has been injected. The analysis shows that the Arbuckle aquifer is leaking significantly at this site. We suggest that the present method may be effective and economical for monitoring leakage in groundwater systems, which bears on the safety of water resources, the security of underground waste repositories, and the outflow of wastewater during deep injection and hydrocarbon extraction.

Plain Language Summary Quantitative interpretation of the tidal response of the hydraulic head of an aquifer has been made either with a model for perfectly confined aquifers or with that for purely unconfined aquifers. However, many aquifers may neither be totally confined nor purely unconfined at the frequencies of tidal loading but behave somewhere between the two end-members. A model for the interpretation of the tidal response of such aquifers, however, is currently lacking. Here we derive a new model for the tidal response of a leaky aquifer and apply the model to interpret the tidal response of water level in a USGS Oklahoma deep monitoring well installed in the Arbuckle aquifer, into which a massive amount of wastewater coproduced from hydrocarbon exploration has been injected. The analysis suggests that the Arbuckle aquifer is leaking significantly at this site. It also shows that Earth tide analysis of water level in wells may be useful for continuous monitoring of leakage of groundwater system, which bears on the safety of water resources, the security of underground waste repositories, and the outflow of wastewater during hydrocarbons extraction.

1. Introduction

The response of aquifers to applied loads, such as Earth tides and barometric pressure, have long been studied for the evaluation of aquifer properties (e.g., Allègre et al., 2016; Hsieh et al., 1987; Roeloffs, 1996; Xue et al., 2016) and their changes after earthquakes (e.g., Elkhoury et al., 2006; Doan et al., 2006; Liao et al., 2015; Zhang et al., 2015). Interpretations of such responses have been made with models either for perfectly` confined aquifers or for purely unconfined aquifers. Most aquifers, however, behave somewhere between these two end-members (Galloway & Rojstaczer, 1989). The vertical impedance to flow across the boundary of a confined aquifer is not infinite, and the response of aquifers to applied load depends on the time scale. With applied loading at low frequencies, a confined aquifer may exchange flow across its boundaries, and at high frequencies, an unconfined aquifer may exhibit some *confined* behaviors. Thus, the analysis of aquifer response to applied loads may benefit from the inclusion of a frequency-dependent leakage.

AGU
100
ADVANCING EARTH
AND SPACE SCIENCE

Water Resources Research

10.1029/2018WR022793

A second motivation for inclusion of leakage in the study of aquifer response to applied loads comes from the coseismic response of water level to earthquakes. Studies have shown that permeability of aquifers may change after earthquakes probably due to seismic shaking that dislodges debris and/or multiphase droplets or bubbles from preexisting fractures (Beresnev & Johnson, 1994; Brodsky et al., 2003; Elkhoury et al., 2006; Liu & Manga, 2009; Manga et al., 2012). If so, one may expect enhanced permeability to occur not only in the horizontal direction but in all directions since the preexisting fractures are likely to be randomly oriented. Furthermore, earthquake-enhanced vertical permeability has been invoked to explain coseismic increases in streamflow (e.g., Wang, Wang, & Manga, 2004; Wang & Manga, 2015), eruption of geothermal water (e.g., Wang, Manga, et al., 2004), changes in groundwater temperature (e.g., Wang et al., 2012, 2013), water shaken out of soils (Mohr et al., 2015) coseismic changes in the tidal response of water levels (Liao et al., 2015; Wang et al., 2016), and migration of seismic swarms (e.g., Ingebritsen & Manning, 2010). Thus, the study of groundwater response to earthquakes may also benefit from the consideration of leakage in the system.

A third motivation for the inclusion of leakage in the study of aquifers is for monitoring the safety of groundwater resource and/or the security of underground repositories. While most aquifers are used as sources of freshwater, some aquifers are used for disposal of wastewater and other hazardous liquids. In either case, it is important to monitor if leakage occurs. For decades massive amounts of wastewater, coproduced from the extraction of oil and gas, have been injected into deep aquifers beneath the U.S. midcontinent (Ellsworth, 2013; Frohlich, 2012; Hornbach et al., 2015; Keranen et al., 2013, 2014; McGarr et al., 2015; Walsh & Zoback, 2015; Weingarten et al., 2015), and disposal activities continue to this day. Concerns arise if the injected fluids can migrate upward and contaminate shallow groundwater (U.S. Environmental Protection Agency, 2016; Vidic et al., 2013); even though such an event has not been documented (Darrah et al., 2014), the issue remains contentious (Vengosh et al., 2014). While continuous monitoring of leakage may be advisable in such situations, traditional methods such as well tests, numerical simulation, and geochemical monitoring are costly and labor intensive—infeasible for continuous monitoring. Here we show that the analysis of the tidal response of water levels in wells provides an effective means for continuous monitoring of leakage in groundwater systems.

As noted earlier, the response of aquifers to Earth tides has been traditionally interpreted either with a model for perfectly confined aquifer or with a model for purely unconfined aquifer. In this study we derive a new analytical solution for the response of groundwater to Earth tides in a leaky aquifer. We apply the model to analyze the tidal response of the water level in a US Geological Survey (USGS) deep monitoring well installed in the Arbuckle aquifer in Oklahoma, where massive amount of wastewater coproduced from hydrocarbon exploration is injected.

2. Previous Studies

The study of groundwater pumping in a leaky system has a long history. Analytical solutions for pumping/injection in leaky, multilayered aquifer systems have been developed since early last century. Hantush and Jacob (1955) and Hantush (1960) considered steady state and transient flow through the aquitard. Solutions were extended to multilayered systems (Cheng, 1994; Cheng & Morohunfola, 1993; Hemker, 1985; Hemker & Maas, 1994; Maas, 1987a, 1987b; Veling & Maas, 2009) and used to investigate pressure change in response to fluid injection or extraction in wells (Cardiff et al., 2013; Cihan et al., 2011; Sun et al., 2015). The study of groundwater response to the solid Earth tide is different from that of groundwater pumping. In the pumping studies, the driving force in a well is treated mathematically as a boundary condition, while in the study of groundwater response to Earth tides the driving force is the poroelastic response to tidal strain. Furthermore, while the study of groundwater pumping in a leaky system has a long history, the study of the response of a leaky groundwater system to the solid Earth tide is at its infancy, as described below.

The classical model of tidal response of groundwater in a confined aquifer by Hsieh et al. (1987) exploits the phase shift caused by the time needed for groundwater in the aquifer to flow into and out of the well; it predicts a negative phase shift of water level oscillation relative to the tidal strain. Another model is for unconfined aquifer with purely vertical flow (Roeloffs, 1996; Wang, 2000), which predicts an apparent positive phase shift of water level oscillation relative to the local tidal volumetric strain. This difference in the sign of phase shift predicted by the two models has been used in previous studies as the primary criterion for deciding whether an aquifer is confined or unconfined and thus which of the above two models should be used in
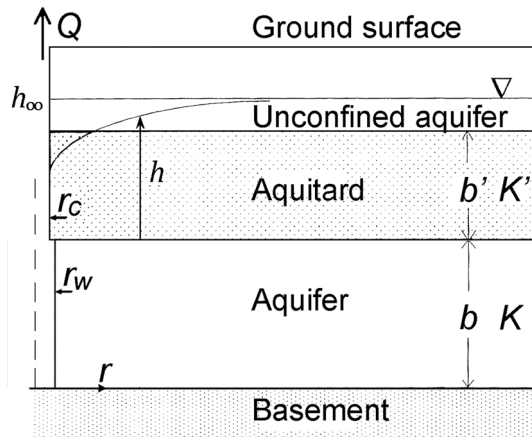
Figure 1. The classical Hantush model for a leaky aquifer. The vertical dashed line on the left shows the position of the well axis located at $r = 0$. The thickness (b) and hydraulic conductivity (K) of the aquifer are related to the aquifer transmissivity by $T = bK$. The equivalent thickness and vertical hydraulic conductivity of the aquitard are b' and K', respectively.

interpreting the tidal response (e.g., Elkhoury et al., 2006; Liao et al., 2015; Zhang et al., 2015; Allègre et al., 2016; Xue et al., 2016). However, many aquifers may neither be perfectly confined nor purely unconfined at the frequencies of tidal loading but behave somewhere between the two end-members. Here we present a more general solution for the response of groundwater to the solid Earth tide with both horizontal flow and vertical leakage. We show that the phase shift may remain negative even when substantial leakage occurs and that positive phase shift may occur only after leakage exceeds some thresholds. Thus, the sign of phase shift, the conventional indicator of a confined aquifer, may not be a reliable criterion for deciding if an aquifer is confined or not.

3. Tidal Response of a Leaky Aquifer

Here we derive the response of the classical leaky aquifer, first introduced by Hantush and Jacob (1955), to the solid Earth tide. The model consists of an aquifer confined above by a semiconfining aquitard that in turn is overlain by an unconfined aquifer (Figure 1). The model applies Darcy's law across the entire aquitard of thickness b' and hydraulic conductivity K' and implicitly assumes that the aquitard is incompressible and has zero storage. The analytical technique for tidal analysis presented below builds upon previous works (Doan et al., 2006; Hsieh et al., 1987) and extends to the classical Hantush leaky aquifer model.

Assuming that the aquifer is laterally extensive and that flow through the semiconfining aquitard is vertical, the tide-induced groundwater flow in the leaky aquifer may be evaluated by solving the following equation:

$$T\left[\frac{\partial^2 h}{\partial r^2} + \frac{1}{r}\frac{\partial h}{\partial r}\right] - \frac{K'}{b'}h = S\left(\frac{\partial h}{\partial t} - \frac{BK_u}{\rho g}\frac{\partial \varepsilon}{\partial t}\right) \tag{1}$$

where h (m) is the hydraulic head in the aquifer above a common reference (Figure 1), r (m) is the radial distance from the studied well, T (m²/s) and S, respectively, are the transmissivity and storativity of the aquifer, ε is the tidal oscillating volumetric strain of the aquifer (compression is taken to be positive), B and K_u (Pa), respectively, are the Skempton's coefficient and the undrained bulk modulus of the aquifer, and K' (m/s) and b' (m), respectively, are the vertical hydraulic conductivity and the thickness of the aquitard. A list of nomenclature is provided in the supporting information. The model in equation (1) differs from the classical model (Hsieh et al., 1987) in its inclusion of the vertical leakage, approximated by $-K'h/b'$ (m/s) and treated mathematically as a volumetric source term, which is justified if the aquifer is relatively thin and the permeability of the aquitard is small (Hantush, 1967). Also implicitly assumed is that the aquitard is incompressible with negligible storage and the flow across it is vertical (e.g., Lee, 1999). These assumptions may be justifiable if leakage through the aquitard is through narrow vertical cracks. The topmost unconfined aquifer is assumed to have high hydraulic conductivity and thus characterized by a hydrostatic head (Hantush & Jacob, 1955; Lee, 1999).

The boundary conditions are

$$h(r,t) = h_\infty(t) \text{ at } r = \infty, \tag{2}$$

$$h(r,t) = h_w(t) \text{ at } r = r_w, \text{ and} \tag{3}$$

$$2\pi r_w T(\partial h/\partial r)_{r=r_w} = \pi r_c^2(\partial h_w/\partial t) \tag{4}$$

where h_w (m) $= h_{w,o}e^{i\omega t}$ is the periodic water level in the well, with complex amplitude $h_{w,o}$ (m); ω [s^{-1}] $= 2\pi/\tau$ is the angular frequency; τ (s) is the period of tidal oscillation; r_w (m) is the radius of the screened portion of the well; and r_c (m) is the inner radius of well casing in which water level fluctuates with tides (Figure 4).

Following Hsieh et al. (1987), we use complex numbers to facilitate the model development below. The solution is obtained by first deriving the response away from the well, h_∞, and then modifying it by considering the effect of the well on aquifer response by using a flux condition at the well that accounts

for wellbore storage. Let the disturbance in water level due to the well be expressed as the negative of *drawdown*, that is,

$$\Delta h(r,t) = h(r,t) - h_\infty(t) \tag{5}$$

where $h_\infty(t)$ (m) is the hydraulic head away from the well (Figure 4a), which is a function of time only and may be evaluated by replacing h by h_∞ in equation (1):

$$-\frac{K'}{b'}h_\infty = S\frac{\partial h_\infty}{\partial t} - \frac{SBK_u}{\rho g}\frac{\partial \varepsilon}{\partial t}. \tag{6}$$

Since h_∞ and ε are both periodic with the same frequency ω, we have

$$h_{\infty,o} = \frac{i\omega S}{i\omega S + K'/b'}\left(\frac{BK_u\varepsilon_o}{\rho g}\right). \tag{7}$$

where $h_{\infty,\,o}$ is the complex amplitude of h_∞ and ε_o the amplitude of ε. It is notable that leakage causes both the amplitude and the phase shift of $h_{\infty,\,o}$ to deviate from that of a perfectly confined aquifer and that $h_{\infty,\,o}$ reduces to that of a perfectly confined aquifer when $K' = 0$.

Replacing h by $\Delta h + h_\infty$ in equations (1) to (4) and using equation (7), we have

$$T\left[\frac{\partial^2 \Delta h}{\partial r^2} + \frac{1}{r}\frac{\partial \Delta h}{\partial r}\right] - \frac{K'}{b'}\Delta h = S\frac{\partial \Delta h}{\partial t}. \tag{8}$$

Since the stationary periodic solution of equation (8) has the form $\Delta h = \Delta h_o(r)e^{i\omega t}$, the above equation may be reduced to an ordinary differential equation

$$T\left[\frac{d^2\Delta h_o}{dr^2} + \frac{1}{r}\frac{d\Delta h_o}{dr}\right] - \frac{K'}{b'}\Delta h_o = i\omega S\Delta h_o. \tag{9}$$

with the boundary conditions

$$\Delta h_o(r\to\infty) = 0, \tag{10}$$

$$\Delta h_o(r = r_w) = h_{w,o} - h_{\infty,o} = h_{w,o} - \frac{i\omega S}{i\omega S + \frac{K'}{b'}}\left(\frac{BK_u\varepsilon_o}{\rho g}\right), \tag{11}$$

$$2\pi r_w T\frac{d\Delta h_o}{dr}\bigg|_{r=r_w} = i\omega\pi r_c^2 h_{w,o}. \tag{12}$$

The solution to equation (9) is $\Delta h_o = C_I I_o(\beta r) + C_K K_o(\beta r)$, where I_o and K_o are, respectively, the modified Bessel functions of the first and second kind and the zeroth order, and

$$\beta = \left(\frac{K'}{Tb'} + \frac{i\omega S}{T}\right)^{1/2}. \tag{13}$$

The boundary condition (equation (10)) asserts that $C_I = 0$; thus, $\Delta h_o = C_K K_o(\beta r)$. Solving for C_K with equation (12) and recalling $\frac{dK_o(r)}{dr} = -K_1(r)$, where K_1 is the modified Bessel function of the second kind and the first order, we have

$$C_K = -\frac{i\omega r_c^2 h_{w,o}}{2T\beta r_w K_1(\beta r)}. $$

Thus,

$$\Delta h_o = -\frac{i\omega r_c^2 h_{w,o} K_o(\beta r)}{2T\beta r_w K_1(\beta r)}. \tag{14}$$

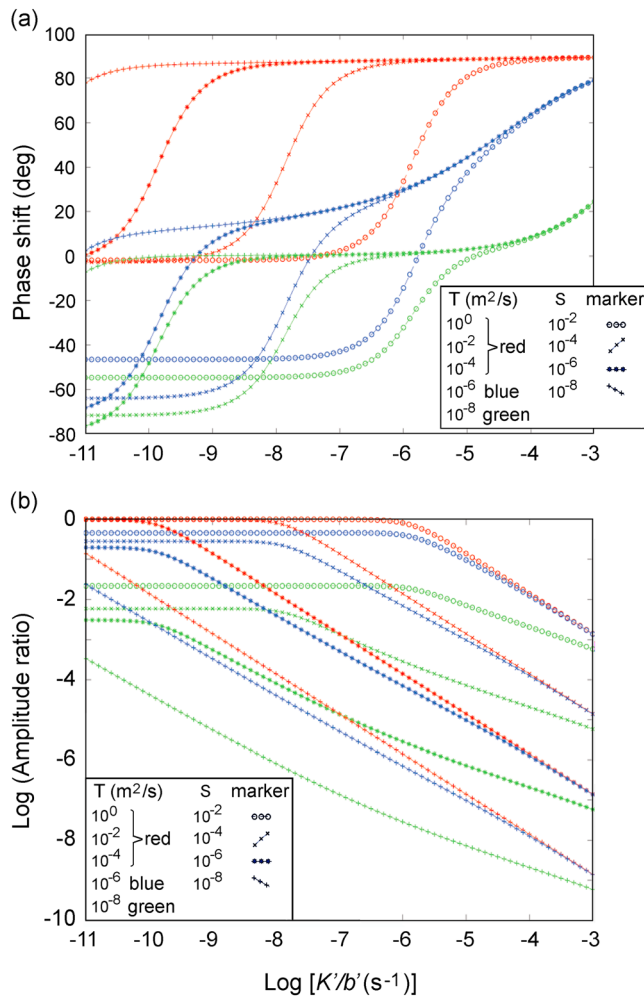Inserting equation (14) into equation (11), we finally have

Figure 2. (a) Phase shift of water level response to the M2 (semidiurnal lunar) tide, plotted against the logarithm of the specific leakage (K'/b') for different T and S, with $r_c = r_w = 10$ cm. Negative values indicate local phase lag. (b) Logarithm of the ratio of the amplitude of water level response to that of the volumetric strain, plotted against the logarithm of K'/b' for different T and S.

$$h_{w,o} = \frac{i\omega S}{(i\omega S + K'/b')\xi}\left(\frac{BK_u\varepsilon_o}{\rho g}\right) \tag{15}$$

where

$$\xi = 1 + \left(\frac{r_c}{r_w}\right)^2 \frac{i\omega r_w}{2T\beta}\frac{K_o(\beta r_w)}{K_1(\beta r_w)} \tag{16}$$

which accounts for the wellbore storage effect. An independent derivation of equation (15) using Laplace transform is given in the supporting information.

The solution has three independent parameters, T and S for the aquifer and K'/b' for the semiconfining aquitard. We define the amplitude ratio of the tidal response as

$$A = \left| h_{w,o} / \left(\frac{BK_u\varepsilon_o}{\rho g}\right) \right|, \tag{17}$$

and the phase shift is defined as

$$\eta = \arg\left[h_{w,o} / \left(\frac{BK_u\varepsilon_o}{\rho g}\right) \right], \tag{18}$$

where arg(z) is the argument of the complex number z. Figure 2 shows plots of the phase shift (η) and the amplitude ratio (A) of the response to the M2 (semidiurnal lunar) tide against K'/b', over broad ranges of aquifer parameters, that is, from 10^{-8} to 1 m²/s for T and from 10^{-8} to 10^{-2} for S. We focus on interpreting the phase shift because the amplitude ratio requires knowledge on K_u and B, that are often unknown or have large uncertainties. We will comment later (section 5.2) on the use of the amplitude ratio for checking the consistency of the model with measurements.

Several aspects of Figure 2 are worthy of notice. First, at $T > 10\text{–}4$ m²/s, the curves for different T and given S collapse onto a single curve (as shown by the red markers). This is because at such high transmissivity, the tidal response of water level in the well becomes identical to the pressure head in the aquifer (e.g., Doan, et al., 2006). Second, with increasing leakage (K'/b'), the phase shift for any pair of T and S changes through a transition from a confined response at relatively low leakage to a unconfined response at relatively high leakage, and the transition occurs at increasing leakage with increasing S. At small K'/b' for constant T and S, the phase shift is constant until K'/b' reaches the lower bound of the transition; thus K'/b' may be estimated only above this lower bound. The amplitude ratio, on the other hand, is nearly constant at leakage below the mid-transition, above which it decreases nearly linearly with log(K'/b'). Third, significant leakage can occur when the phase shift is negative. For example, if $T = 10\text{–}6$ m²/s and $S = 10\text{–}6$, a phase shift of $-20°$ would predict a specific leakage of $K'/b' \sim 10\text{–}10$ s^{-1} (Figure 2). If b' (aquitard thickness) is ~100 m, the corresponding K' (vertical conductivity of the aquitard) is ~10-8 m/s. Thus, negative phase shift in the tidal response may not be an indicator of good confinement and consideration of aquifer leakage is required. Fourth, phase shift becomes positive at large K'/b'; the threshold of K'/b' at which phase shift becomes positive depends upon T and S; at fixed T, this threshold decreases significantly with decreasing S.

An exhaustive verification of the solution for a leaky aquifer (15) against other analytical models cannot be made because no such model is available in publication. Thus, we compare the solution at its end conditions (i.e., purely horizontal and purely vertical flows) against the model of a confined aquifer and that of an unconfined model.
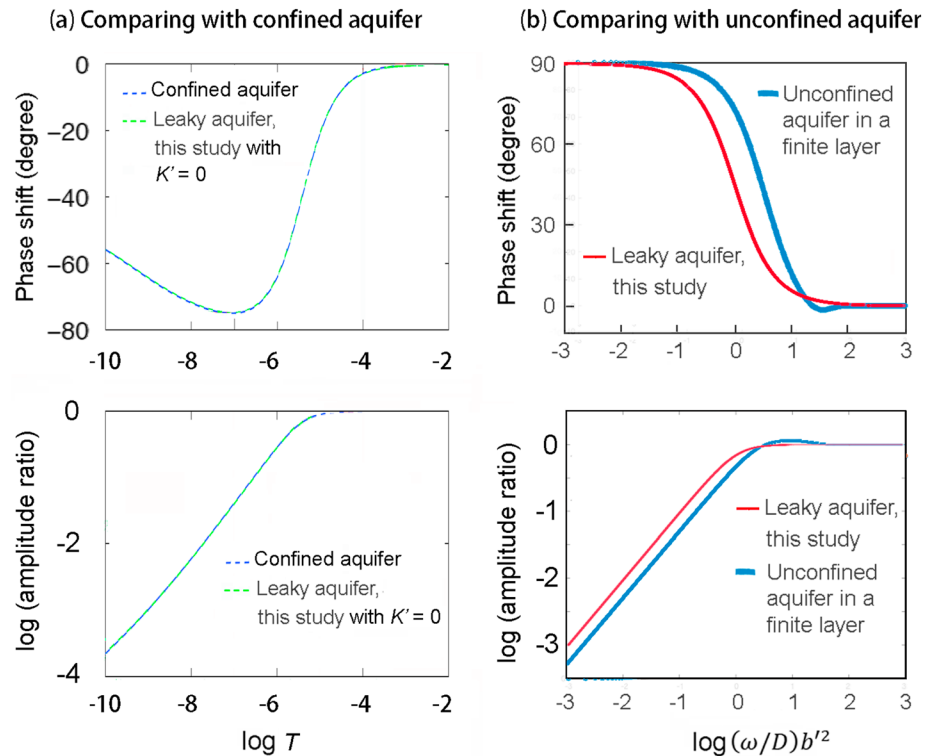
Figure 3. (a) Phase shift and amplitude ratio of water level response to the M2 tide predicted by the present model with $K' = 0$, compared with that predicted by a perfectly confined aquifer (Doan et al., 2006; Hsieh et al., 1987). (b) Phase shift and amplitude ratio of water level response to the M2 tide predicted by the present model (equation (21)) and the model of unconfined aquifer in a finite layer (equation (20)) plotted against $(\omega/D)b'^2$.

We may compare the solution against that for a confined aquifer by setting $K' = 0$, which reduces equation (15) to

$$h_{wo} = \frac{BK_u\varepsilon_o}{\rho g}\frac{1}{\xi}\bigg|_{K'=0},$$ (19)

which is identical to the classical solution for a perfectly confined aquifer (Doan et al., 2006; Hsieh et al., 1987). Figure 3 further shows the predicted phase shift and amplitude ratio for the M2 tide by equation (15) at $K' = 0$, which match seamlessly with those predicted by a perfectly confined aquifer.

We may also compare the solution (equation (15)) against that for an unconfined aquifer away from the well ($r \to \infty$) where horizontal flow is zero and $h_{\infty, o}$ is given by equation (7). Since the present model is confined below (Figure 1), the comparison is made with the model for unconfined aquifers in a finite layer (Detournay & Cheng, 1993),

$$\frac{\rho g h_o}{BK_u\varepsilon_o} = 1 + \tanh\lambda \sinh\left(\frac{\lambda z}{L}\right) - \cosh\left(\frac{\lambda z}{L}\right)$$ (20)

where L is the thickness of the layer, $\lambda \equiv L\sqrt{i\omega/D}$, and z is the depth of the screening interval of a cased well. Expressing equation (7) in the same form, we have

$$\frac{\rho g h_{\infty,o}}{BK_u\varepsilon_o} = \frac{i\omega S}{i\omega S + K'/b'} = \frac{i\omega b'^2/D}{(i\omega b'^2/D) + 1},$$ (21)

where $D = K_s/(S/b')$. Equations (7) and (20) share the common variable ω. Plotting their predicted phase shift and amplitude ratio (with $L = z = b'$) against $(\omega/D)b'^2$ (i.e., the dimesionless frequency; Galloway & Rojstaczer,
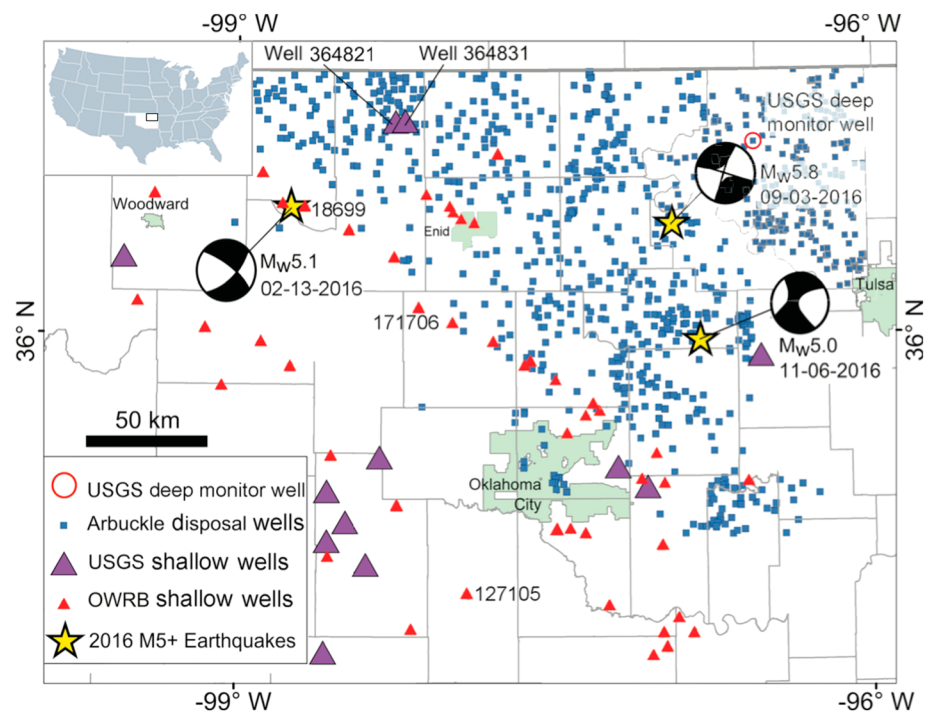
Figure 4. Location of the USGS Oklahoma deep monitoring well (red circle on top right corner), together with the locations of Arbuckle disposal wells, shallow USGS and OWRB (Oklahoma Water Resources Board) monitoring wells, and the epicenters of large earthquakes in 2016. Inset map on upper left of diagram shows the study area (small rectangle) in the State of Oklahoma (white polygon).

1989) in Figure 4b, we show that the present model is also in good agreement with the unconfined aquifer model in a finite layer.

4. Application of the Leaky Aquifer Model to the Arbuckle Aquifer, Oklahoma

For decades, massive amounts of wastewater have been injected into the deeply buried part of the Arbuckle aquifer of Oklahoma, but volumes have increased substantially in the last decade. The injection has caused dramatic increases in seismicity rate (Ellsworth, 2013; McGarr et al., 2015; Walsh & Zoback, 2015; Weingarten et al., 2015), including several $M \geq 5$ earthquakes (Barbour et al., 2017; Keranen et al., 2013, 2014; McNamara et al., 2015; Yeck et al., 2016; Yeck et al., 2016; see Figure 4 for locations of disposal wells and epicenters of major earthquakes in 2016). In April 2017 the U.S. Geological Survey (USGS) installed a pressure gauge in a deep monitoring well in the Arbuckle aquifer in northeastern Oklahoma (see Figure 4 for well location with respect to injection wells and Table 1 for detailed well information), measuring water levels continuously at a rate of one sample per minute.

The Arbuckle formation is a thick deposit of laterally extensive, dominantly Late Cambrian to Early Ordovician limestone and dolomite over a Proterozoic to Early Cambrian igneous basement in the U.S. midcontinent (Johnson, 2008). During the Late Carboniferous period the aquifer was deformed, uplifted, eroded, and exposed in south central Oklahoma. Beneath north central Oklahoma, however, this aquifer is deeply buried and confined by younger formations (Johnson, 2008). It is generally accepted that the hydraulic communication between the buried Arbuckle aquifer and its exposed outcrops following the uplift and erosion is the principal cause of underpressure in the Arbuckle aquifer (Sorenson, 2005).

The well log in Figure 5 shows that the Arbuckle aquifer near the USGS deep monitoring well is confined by a sequence of sedimentary strata including a basal shale, sandstones, and carbonate rocks, which in turn is overlain by an unconfined aquifer of younger sediments. This stratigraphic sequence corresponds closely with the conceptual model of Hantush and Jacob (1955) for a leaky aquifer described above (Figure 1), with the sequence of basal shale, sandstone, and carbonate rocks above the Arbuckle aquifer (Figure 5) representing the semiconfining aquitard.

Table 1
Parameters of the USGS Oklahoma Deep Well and the Hydrogeological Parameters Used in Estimating the Vertical Conductivity of the Leaking Aquitard

Parameters	Symbol	Values	References
Well location and elevation		36.7269°N, 96.5317°W 340.16 m above sea level	USGS website[a]
Well depth		960 m beneath surface	This study
Well radius	r_w	11 cm	This study
Casing radius	r_c	3.65 cm	This study
Thickness of aquitard	b'	277 m	Figure 5
Thickness of aquifer	b	48 m	Figure 5
Permeability[d]	k	2×10^{-14} to 3×10^{-12} m^2	Morgan and Murray (2015)
Transmissivity[b]	T	9.6×10^{-6} to 1.4×10^{-3} m^2/s	Calculated from k
Specific storage	S_s	5.4×10^{-8} to 5.6×10^{-7} m^{-1}	Rahi and Halihan (2009)
Storativity[c]	S	2.6×10^{-6} to 2.7×10^{-5}	Calculated from S_s

[a]https://waterdata.usgs.gov/nwis/uv/?site_no=364337096315401.   [b]Transmissivity is calculated from permeability using the relationship $T = b(\rho g k/\mu)$, where ρ and μ are, respectively, the density and viscosity of pore fluid in the Arbuckle aquifer. As explained in the text, groundwater in the Arbuckle aquifer near the USGS well is similar to freshwater; thus, we take $\rho = 1{,}000$ kg/m^3 and $\mu = 0.001$ Pa/s in the calculation of T from k.   [c]Storativity S is calculated from specific storage S_s (Rahi & Halihan, 2009) using the relationship $S = bS_s$.   [d]Permeability was measured on the outcrop surface and core measurements. We use the median to maximum range of measured values because small-scale matrix permeability represents the lower end of permeability for the Arbuckle aquifer (Morgan & Murray, 2015).

4.1. Tidal Response of Water Level in the USGS Monitoring Well

Water level in the USGS Oklahoma deep monitoring well is measured with a pressure sensor LevelTROLL 500 manufactured by in situ (https://in-situ.com/wp-content/uploads/2014/11/SS_LevelTROLL_Spec_Sheet_Dec2017.pdf). It is a vented, piezoresistive transducer made of titanium, with a nominal accuracy of 0.05% full scale. The signal is digitized at the surface at a sampling rate of 1/4 Hz, low-pass filtered to 1-min sampling, and sent by satellite telemetry to the U.S. National Water Information System.

We use the code Baytap08 (Tamura et al., 1991) for extracting tidal signals from the data. The method is based on Bayesian statistics with the prior knowledge that the time series comprises tidal components with known periods and a drift that includes long-period and secular changes. Figure 6 shows the time series of raw data for water level above the mean sea level in the USGS Oklahoma deep monitoring well. Figures 6b to 6c show, respectively, the drift that was removed and the remaining tides used in the analysis. There is no meteorological station at or very near the well; thus, the barometric effect on water level is not corrected and we focus on the response to the M2 tide because it is minimally affected by changes in the barometric pressure. The effect of ocean loading at the USGS well is small because of the large distance of the well from the coasts; calculations using SPOTL (a software for modeling the response to ocean-tide loading; Agnew, 2012) show that the ocean-tide effect is ~5% of that of the solid Earth tide.

The period of the M2 tide (0.5175 day) is close to that of the S2 (semidiurnal solar) tide (0.5000 day), and spectral leakage between the S2 and the M2 tides can pose challenges for tidal analysis (Allègre et al., 2016). We choose a window size of 29.5036 days, the minimum time window needed to separate the frequencies of the semidiurnal M2 and S2 tides (Allègre et al., 2016; Xue et al., 2016). Figure 6d shows the time-varying phase shift of water level response to the M2 and S2 tides, referenced to the local volumetric strain tides. Negative phase shift indicates phase lag, and positive indicates phase advance. The root-mean-square errors for the determinations are ~0.3°, on average. Large and variable changes in the phase shift of the S2 tide are probably due to changes in barometric
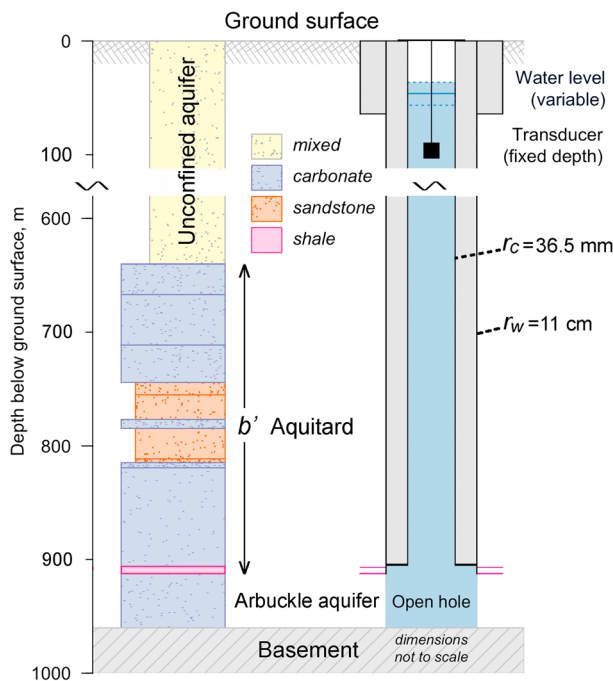

Figure 5. Simplified completion diagram of the USGS Oklahoma deep monitoring well. The Arbuckle aquifer is the lowest sedimentary rock that lies above the basement. Comparing with the conceptual model in Figure 1, the sequence of sedimentary rocks between the Arbuckle aquifer and the topmost unconfined aquifer, which includes a basal shale, sandstone, and carbonate, makes up the aquitard. The unconfined aquifer consists of unconsolidated sediments.
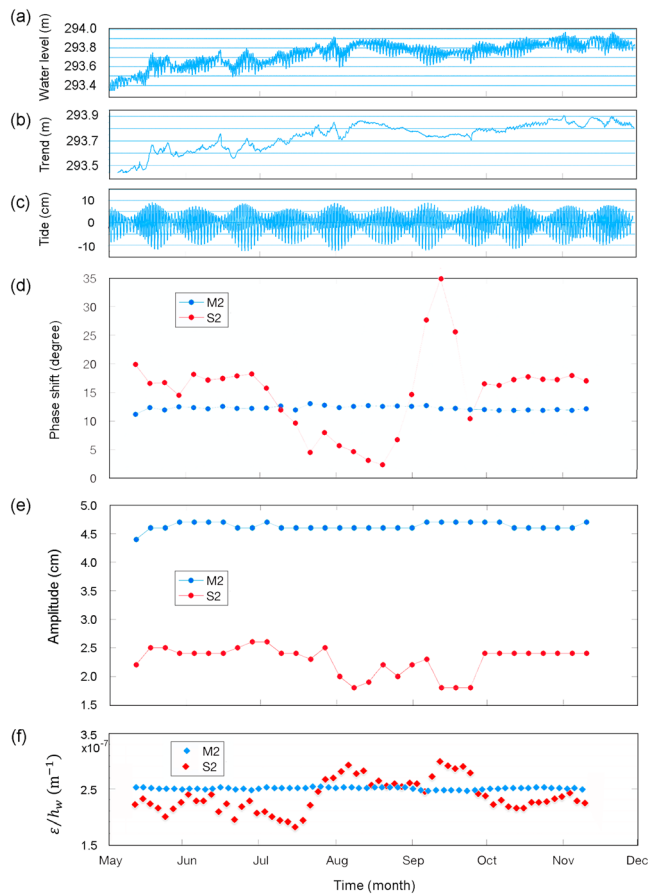
Figure 6. Time series of (a) raw data for water level above the mean sea level in the USGS Oklahoma deep monitoring well, (b) drift that was removed, (c) remaining tides in water level used in the analysis, (d) phase shift of water level response to the M2 and S2 tides referenced to the local tidal volumetric strain, (e) amplitude of water level response to the M2 and S2 tides, and (f) response of $\varepsilon_o/h_{w,o}$ to the M2 and S2 tides, where ε_o is the amplitude of the volumetric strain converted from surface strain computed in Baytap08.

pressure and temperature, whereas the phase shift of the M2 tide is positive and stable at ~12.5° throughout the studied period: these two tidal constituents are well separated in the analysis. The amplitude response of water level to the M2 tide is also stable at ~4.5 cm (Figure 6e), while that of the S2 tide shows considerable variability.

4.2. Interpretation of the Tidal Response

As noted earlier, both geologic studies (e.g., Johnson, 2008) and well logs (e.g., Figure 5) show that the Arbuckle aquifer is confined—an ideal target for massive injection of wastewater. Thus, the positive phase shift of water level from the above analysis (Figure 6d) was unexpected and suggests that the confining units of the Arbuckle near the USGS deep well may be leaking. In this section we use the model for a leaky aquifer derived in section 3 to interpret the tidal response of the Arbuckle aquifer with data from the USGS Oklahoma deep monitoring well (Figure 6). Table 1 lists the other hydrogeological parameters for the Arbuckle aquifer needed to interpret the measured phase shift from tidal analysis. In particular, the permeability (k) measured on core samples of the centimeter scale from the Arbuckle aquifer (Morgan & Murray, 2015) shows a range from 2×10^{-14} to 3×10^{-12} m^2, and the specific storage (S_s) obtained from tidal analysis of groundwater level in south central Oklahoma (Rahi & Halihan, 2009) shows a range from 5.4×10^{-8} to 5.6×10^{-7} m^{-1}. For the inference of the groundwater leakage we use the median-to-maximal range of the measured permeability because small-scale matrix permeability most likely represents the lower end of permeability for the Arbuckle aquifer. These parameters are related to T and S by the following relations, respectively, $k = (\mu/\rho g b)T$ and $S_s = S/b$, where g is the gravitational acceleration and ρ and μ are, respectively, the density and viscosity of pore fluid in the Arbuckle aquifer. Given the open hole thickness of 48 m in the USGS well, the range of S_s corresponds to a range of S from 2.6×10^{-6} to 2.7×10^{-5} and the range of k corresponds to a range of T from 9.6×10^{-6} to 1.4×10^{-3} m^2/s. The use of data from core-scaled samples instead of field-scaled data is due to the scarcity of the latter; measurement of T and S at field scale is needed for better interpretation of the measured phase shift at the USGS deep monitoring well.

Figure 7a shows the model curves (equation (15)) for the phase shift in the M2 tide versus log(K'/b'), for the range of T and S in Table 1. For a given value of S, the curves lie close together for the realistic range of T; however, for a given value of T, the curves for the realistic range of S (Table 1) lie apart. Figure 7b shows the model curves (equation (14)) for amplitude ratio versus log(K'/b') for the range of T and S in Table 1; here the curves for the range of T overlap at a given S.

The phase shift of 12.5° for the water level response to the M2 tide in the USGS well (Figure 2d), represented by a purple horizontal line in Figure 7a, intersects the model curves at K'/b' of 10^{-10} to 10^{-9} s^{-1} for $S = 2.6 \times 10^{-6}$ to 2.7×10^{-5}. Given the thickness of 277 m for the semiconfining aquitard (Table 1), these values correspond to $K' \sim 3 \times 10^{-8}$ to 3×10^{-7} m/s, respectively. As shown in the next section, this result provides the basic evidence that the Arbuckle aquifer is leaking.

5. Discussion

Several aspects of the above analysis are discussed below, including the assessment and verification of the leakage of the Arbuckle aquifer, the estimate of the leakage rate, the electrical conductivity and water level in the USGS deep well, and the criteria for separating the leakage effect on tidal response from that of enhanced horizontal permeability.
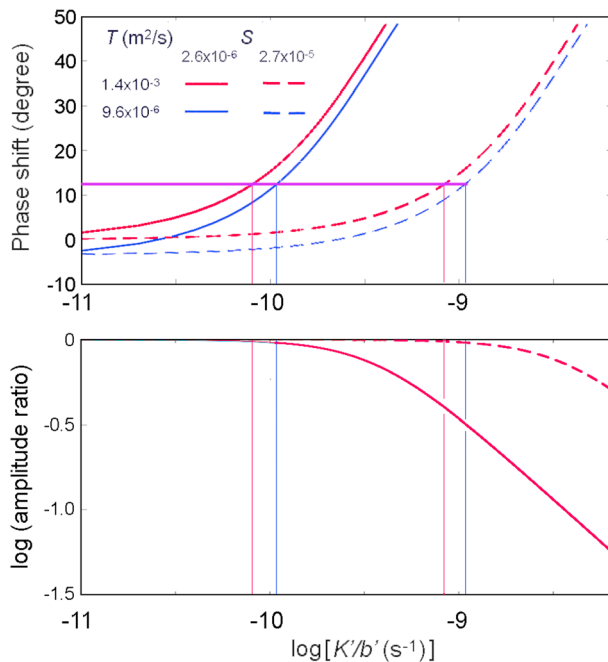
Figure 7. (a) Calculated phase shift of water level response for the M2 tide as a function of K'/b' (colored curves) with predetermined values of T and S (Table 1). The values of rc and rw used in the calculation are as specified on the completion diagram (Figure 4). The horizontal line shows the observed phase shift in the USGS well, where it intersects with model curves (vertical lines) give K'/b' of the aquitard. (b) Calculated amplitude ratio of water level response to M2 tide as a function of K'/b' (colored curves). Curves calculated with different values of T at equal S overlap on this diagram. The estimated K'/b', from (a), intersect the amplitude ratio curves at ~1.

5.1. Assessment on Leakage of the Arbuckle Aquifer

We may examine the hydraulic integrity of the aquitard above the Arbuckle aquifer by comparing the above estimated K' with that of a hypothetical, intact aquitard consisting of the same strata as shown in the well log (Figure 5), each assigned with a representative hydraulic conductivity according to its lithology. The average vertical hydraulic conductivity of a sequence of horizontal layers may be estimated from the harmonic mean of the vertical hydraulic conductivity of the individual layers (Ingebritsen et al., 2006), that is, $K' = b'/\sum_i (b_i/K_i)$, where K_i is the vertical hydraulic conductivity of the ith layer in the aquitard. This relation shows that the average vertical conductivity of the horizontal layers in the aquitard is controlled by the layer with the lowest conductivity. Table 2 lists the thickness of each individual layer in the aquitard and its representative hydraulic conductivity, assigned according to the intact rock of the lithology of the layer. The calculated average vertical hydraulic conductivity of the hypothetical aquitard is ~5×10^{-12} m/s and is controlled by the 6-m-thick intact shale. This conductivity is many orders of magnitude lower than that estimated from tidal analysis (10^{-8} to 10^{-7} m/s). The basal shale of the aquitard would need to have a vertical hydraulic conductivity many orders of magnitude greater than that of intact (unfractured) shale in order to raise the calculated average vertical conductivity to the same order as that determined from tidal analysis. We therefore conclude that the basal shale above the Arbuckle aquifer near the USGS well is leaking, due perhaps to the presence of conductive fractures.

Massive injection of wastewater in the central and eastern U.S. has caused a surge of induced earthquakes in and near the injection area. Analyses of coseismic changes in stream discharge (Manga et al., 2016) and groundwater level (Wang et al., 2017) in Oklahoma after some $M > 5$ earthquakes suggest that such hydrological responses may be caused by increased crustal permeability, which in turn reflects a coseismic increase of hydraulically conductive fractures. Since the USGS well is located near some of the large ($M > 5$) induced earthquakes (e.g., Figure 4), it may be reasonable to hypothesize that induced seismicity may have played a role in forming conductive fractures in the basal shale, as suggested from the above analysis, even though no direct evidence is available because we lack water level data from the USGS well prior to these earthquakes. However, this could be tested in the future if a strong-to-moderate-magnitude earthquake occurs near the monitoring well.

5.2. Verification of the Leakage Assessment

Although there is no independent evidence near the USGS well to corroborate the result that the Arbuckle is leaking, hydrogeological simulations of groundwater flow in south central Oklahoma (Christenson et al.,

Table 2

Thickness and Assumed Permeability of Rocks in Calculating the Harmonic Mean of Vertical Permeability of a Hypothetical, Hydraulically Intact Aquitard

Rock layer	Thickness (m)	Vertical hydraulic conductivity (m/s)	Reference
Carbonate	106	10^{-6}	Morgan and Murray (2015)
Sandstone	31	10^{-8}	Wang (2000)
Carbonate	9	10^{-6}	Morgan and Murray (2015)
Sandstone	28	10^{-8}	Wang (2000)
Carbonate	92	10^{-6}	Morgan and Murray (2015)
Shale	6	10^{-13}	Wang (2000) (for Piere shale)

2011) show that significant vertical conductivities of the layers above the Arbuckle aquifer are required to fit observational data.

We may also test the consistency of the above result against existing laboratory measurements of rock properties. Figure 6b shows that the amplitude ratios of the tidal response of water level in the USGS deep well are ~1 for the range of K'/b' estimated above and the relevant T and S (Table 1). Thus, $h_{w, o} \approx BK_u\varepsilon_o/\rho g$, where ε_o is the amplitude of the oscillating volumetric strain in response to the M2 tide. From tidal analysis we have $h_{w, o} \approx 0.045$ m (Figure 6e). With ε_o converted from the theoretical surface strain using a Poisson ratio of 0.25, we have $\varepsilon_o/h_{w, o} \approx 2.5 \times 10^{-7}$ m^{-1} (Figure 6f). Thus, BK_u ~40 GPa, which falls close to the upper bound of the range of published values for consolidated rocks from laboratory measurements (Table C1 in Wang, 2000).

Kroll et al. (2017) estimate the poroelastic parameters for the Arbuckle formation based on the analysis of the coseismic response of water levels in similar deep wells to large ($M \geq 5$) induced earthquakes in Oklahoma. Their approach assumes that the coseismic water level response is caused by static volumetric strain estimated from a dislocation model with a set of earthquake source parameters. However, Wang et al. (2017) showed that most measured coseismic volumetric strains disagree with that calculated from the dislocation model. Thus, additional mechanisms may play a role in determining the coseismic volumetric strain.

5.3. Estimate the Leakage Rate

Given the value of K'/b' from tidal analysis, we may estimate the rate of leakage across the aquitard near the USGS deep well. Figure 6a shows that the average hydraulic head of the Arbuckle aquifer was ~293.6 m above sea level (asl) during the time of this study, or ~46.6 m beneath the ground surface, given the ground elevation at the well (Table 1). Although there is no shallow well data near the USGS well, the water table in Oklahoma is mostly near the surface (Wang et al., 2017). Thus, the current leakage of groundwater near the USGS site is downward into the Arbuckle aquifer, rather than out of the aquifer. Since pore pressure in the unconfined aquifer is likely to be hydrostatic, as noted earlier, we may estimate the rate of leakage by $K'h/b'$ where $h \sim 46.6$ m. Given the range of K'/b' estimated from the above tidal analysis (i.e., 10^{-10} to 10^{-9} s^{-1}), we estimate a downward leakage of groundwater from the unconfined aquifer into the Arbuckle at a rate of 4.7×10^{-9} to 4.7×10^{-8} m/s (or 0.15 to 1.5 m/yr) near the USGS deep monitoring well.

Water level in the Arbuckle aquifer shows significant secular change with time (Figure 6b). Could this change be related to the downward leakage from the unconfined aquifer to the Arbuckle? The average rate of water level increase in the USGS deep well was ~1.5 m/yr between May and August 2017 (Figure 2b), similar to the upper bound of the estimated downward leakage. Between August and December 2017, however, the average rate of water level increase is nearly zero (Figure 6b). Furthermore, the timing of the change in the rate of water level change does not correspond to that of the change in the injection rate in the well. Thus, further testing of this hypothesis is needed with longer monitoring of water level in the well.

Another possible leak is into the igneous basement beneath the Arbuckle aquifer, which is not discussed in this study. The contact between the Arbuckle and the basement is an unconformity and likely to be hydraulically conductive. Most induced earthquakes in Oklahoma occur in the basement (e.g., Schoenball & Ellsworth, 2017), suggesting that some injected fluid must have leaked into the basement (Barbour et al., 2017; Zhang et al., 2013). The size of this leak is difficult to estimate but is likely to be small in view of the small porosity of the basement rocks.

5.4. Electrical Conductivity and Water Level in the USGS Deep Well

The specific electrical conductivity of groundwater in the USGS deep monitoring well was measured in April of 2017 and lies between 0.005 and 0.05 S/m. Since the USGS deep monitoring well is cased from the surface to the top of the Arbuckle aquifer (Figure 5), water in the well comes solely from the Arbuckle aquifer. This measured specific electrical conductivity of the groundwater is within the range for freshwater, which is unexpected because it is at least an order of magnitude lower than the specific electrical conductivity of the flow-back fluids commonly injected (e.g., Edwards et al., 2011; Li et al., 2014).

Several mechanisms may have operated to dilute the concentration of the injected fluid. First is the dilution by the lateral dispersion of the injected brine by the tidally induced groundwater flow between the well and the aquifer. Available records show that a total of 926 bbl (~150 m^3) of brine was injected in this well in October and November of 2014 and otherwise none. Numerical simulation would be required for a

detailed investigation of the dispersion of the injected brine with time, which is outside the scope of this study. Instead, we offer the following order-of-magnitude estimate of the degree of dilution of the injected fluid.

Tidal oscillations of water level in the well induce lateral groundwater flow between the well and the aquifer. The length scale associated with this back-and-forward flow may also signify where effective advective mixing occurs between the injected fluid and groundwater and may be estimated as follows. Darcy's law states that the flow rate is proportional to the gradient in the hydraulic head ($\frac{d\Delta h_o}{dr}$). From equation ((14)), we then find that the flow rate decreases with distance as

$$\frac{d\Delta h_o}{dr} = \frac{d[C_K K_o(\beta r)]}{dr} = -\beta C_K K_1(\beta r) \tag{22}$$

where β is given by equation (13). The length scale controlling the flow rate is thus

$$L = \frac{|\Delta h_o|_{max}}{\left|\frac{d\Delta h_o}{dr}\right|_{max}} = \frac{1}{\beta} = \left\{ T/\left[\left(K'/b' \right)^2 + (\omega S)^2 \right]^{1/2} \right\}^{1/2} \tag{23}$$

where $\omega = 2\pi/\tau$ is the angular frequency of the tidal oscillation and $\tau = 0.5175$ day is the period of the M2 tide. Given the values for K'/b' estimated earlier and for T and S listed in Table 1, we estimate $L \sim 100$ m around the USGS deep well. In addition, given the long duration (~3 years) between the brine injection and the conductivity measurement, we make the simplifying assumption that mixing between the injected brine and groundwater in the aquifer is so effective that the concentration within a radius L around the well is uniform at the time of the conductivity measurement. Assuming an average porosity of 0.1 for the Arbuckle aquifer, the total pore volume in the aquifer within a radius of 100 m around the well is $\sim 1.5 \times 10^5$ m^3. Thus, the injected brine is diluted by a factor of $\sim 10^{-3}$ due to mixing with groundwater by the tidally induced oscillating flow.

A second mechanism is the downward leakage of groundwater from the unconfined aquifer to the Arbuckle aquifer discussed in the above section. At a rate of 0.15 to 1.5 m/yr, the downward leakage between the end of injection and the time of conductivity measurement would have added an average amount of freshwater of ~0.4 to 4 m^3/m^2 to the Arbuckle aquifer. Given that the average pore volume per unit area is 4.8 m^3/m^2, the average concentration of pore water at the time of conductivity measurement would have been further diluted by as much as a factor of 2 by downward leakage of freshwater.

A third mechanism is dispersion of the injected fluid by groundwater flow in the Arbuckle aquifer. However, since there is no information about the velocity of groundwater flow near the USGS deep monitoring well, quantitative test of the hypothesis is difficult.

5.5. Separating Leakage Effect From that of Enhanced Permeability

As noted earlier, considerable leakage of a confined aquifer may occur at negative phase shift. Thus, it may be challenging to separate the effect of enhanced horizontal permeability on the tidal response of a confined aquifer from the effect of increased vertical leakage. For the tidal response of a confined aquifer, the increase in phase shift due to an enhancement of the horizontal permeability is associated with an increase in the amplitude ratio (Doan et al., 2006; Hsieh et al., 1987). On the other hand, the increase of phase shift due to increased vertical leakage is associated with a decrease in the amplitude ratio (Figures 2 and 6). Thus, changes in both the phase and amplitude ratio are needed in order to differentiate between the effect of enhanced horizontal permeability and that of increased vertical leakage. If permeability increases in both directions, a large increase in phase shift may be associated with a reduced amplitude ratio.

Another interesting question is related to the separation of the leakage effect from that of enhanced vertical permeability. Since the solution of the vertical flow in a finite unconfined aquifer is comparable to the solution of the leaky aquifer model (Figure 3b), how do we separate the model of an unconfined aquifer in a finite layer from the present model? As explained in the text, both geological studies and well logs show that the Arbuckle aquifer is confined on the top, and the leaky aquifer model deals with the leakage in the confinement, while the unconfined aquifer model discounts the evidence for the existence of the confinement

Finally, we call attention to the simplifications made in the model (Hantush, 1967) that limit its applicability to aquifers with relatively small thickness and leakage. Furthermore, the effects of many geologic complexities such as local topography (e.g., Galloway & Rojstaczer, 1989) and fracture flow (e.g., Bower, 1983) have not been considered. Although the model is simple, the results presented here are robust in that vertical leakage may have occurred in the Arbuckle groundwater system. Continued injection of large quantities of wastewater into this aquifer may have caused its hydraulic head to increase with time (Figure 6b); thus, continued monitoring of water level in this well may be necessary in order to provide timely warning on possible reversal of the current direction of leakage in the Arbuckle aquifer. Additionally, this study suggests that tidal-based detection of groundwater leakage can be useful for continuously monitoring the safety of a groundwater source, seepage from nuclear waste repository, and outflow of wastewater during hydrofracking. The method may also be used for the detection of earthquake-induced groundwater leakage (e.g., Wang et al., 2016) by comparing water level responses to Earth tides before and after an earthquake.

References

Agnew, D. C. (2012). SPOTL: Some programs for ocean-tide loading, SIO technical report, Scripps Institution of Oceanography, UC San Diego, Calif. Retrieved from http://escholarship.org/uc/sio_techreport

Allègre, V., Brodsky, E. E., Xue, L., Nale, S. M., Parker, B. L., & Cherry, J. A. (2016). Using earth-tide induced water pressure changes to measure in situ permeability: A comparison with long-term pumping tests. *Water Resources Research*, *52*, 3113–3126. https://doi.org/10.1002/2015WR017346

Barbour, A. J., Norbeck, J. H., & Rubinstein, J. L. (2017). The effects of varying injection rates in Osage County, Oklahoma, on the 2016 M_w 5.8 Pawnee earthquake. *Seismological Research Letters*, *88*(4), 1040–1053. https://doi.org/10.1785/0220170003

Beresnev, I. A., & Johnson, P. A. (1994). Elastic wave stimulation of oil production: A review of methods and results. *Geophysics*, *59*, 1000–1017.

Bower, D. R. (1983). Bedrock fracture parameters from the interpretation of well tides. *Journal of Geophysical Research*, *88*(B6), 5025–5035. https://doi.org/10.1029/JB088iB06p05025

Brodsky, E. E., Roeloffs, E., Woodcock, D., Gall, I., & Manga, M. (2003). A mechanism for sustained ground water pressure changes induced by distant earthquakes. *Journal of Geophysical Research*, *108*(B8), 2390. https://doi.org/10.1029/2002JB002321

Cardiff, M., Barrash, M., & Kitanitis, P. K. (2013). Hydraulic conductivity imaging from 3D transient hydraulic tomography at several pumping/observation densities. *Water Resources Research*, *49*, 7311–7326. https://doi.org/10.1002/wrcr.20519

Cheng, A. H.-D. (1994). Reply to "Comment on 'Multilayered leaky aquifer systems: 1. Pumping well solutions' by A. H.-D. Cheng and O. K. Morohunfola". *Water Resources Research*, *30*(11), 3231. https://doi.org/10.1029/94WR01803

Cheng, A. H.-D., & Morohunfola, O. K. (1993). Multilayered leaky aquifer systems: Pumping well solutions. *Water Resources Research*, *29*(8), 2787–2800. https://doi.org/10.1029/93WR00768

Christenson, S., Osborn, N. I., Neel, C. R., Faith, J. R., Blome, C. D., Puckette, J., & Pantea, M. P. (2011). *Hydrogeology and simulation of groundwater flow in the Arbuckle-Simpson aquifer, south-central Oklahoma* (pp. 2011–5029). Reston, VA: U.S. Geol. Surv. Sci. Invest. Rept.

Cihan, A., Zhou, Q., & Birkholzer, J. T. (2011). Analytical solutions for pressure perturbation and fluid leakage through aquitards and wells in multilayered-aquifer systems. *Water Resources Research*, *47*, W10504. https://doi.org/10.1029/2011WR010721

Darrah, T. H., Vengosh, A., Jackson, R. B., Warner, N. W., & Poreda, R. J. (2014). Noble gases identify the mechanisms of fugitive gas contamination in drinking-water wells overlying the Marcellus and Barnett shales. *Proceedings of the National Academy of Sciences of the United States of America*, *111*(14), 076–14,081.

Detournay, E., & Cheng, A. H.-D. (1993). Fundamentals of poroelasticity. In J. A. Hudson (Ed.), *Comprehensive rock engineering: Principles, practice and projects*, (Vol. 2, pp. 113–171). Oxford, UK: Pergamon Press.

Doan, M. L., Brodsky, E. E., Prioul, R., & Signier, C. (2006). Tidal analysis of borehole pressure: A tutorial, Schlumberger-Doll Research Report, Cambridge, Mass. Retrieved from https://isterre.fr/IMG/pdf/tidal_tutorial_SDR.pdf

Edwards, P. J., Tracy, L. L., & Wilson, W. K. (2011). Chloride concentration gradients in tank-stored hydraulic fracturing fluids following flowback, U.S. Dept. Agriculture, Research Paper-NRS-14.

Elkhoury, J. E., Brodsky, E. E., & Agnew, D. C. (2006). Seismic waves increase permeability. *Nature*, *411*, 1135–1138.

Ellsworth, W. L. (2013). Injection-induced earthquakes. *Science*, *341*(6142). https://doi.org/10.1126/science.1225942

Frohlich, C. (2012). Two-year survey comparing earthquake activity and injection-well locations in the Barnett Shale, Texas. *Proceedings of the National Academy of Sciences of the United States of America*, *109*(13), 934–13,938.

Galloway, D. L., & Rojstaczer, S. A. (1989). Inferences about formation elastic and fluid flow properties from the frequency response of water levels to atmospheric loads and earth tides: 4th Canadian/American conference on hydrogeology: Fluid flow. *Heat Transfer and Mass Transport in Fractured Rocks, Banff, Alberta, Canada, June, 21-24*(1988), 100–113.

Hantush, M. S. (1960). Modification of the theory of leaky aquifers. *Journal of Geophysical Research*, *65*(11), 3713–3725. https://doi.org/10.1029/JZ065i011p03713

Hantush, M. S. (1967). Flow of groundwater in relatively thick leaky aquifers. *Water Resources Research*, *3*(2), 583–590.

Hantush, M. S., & Jacob, C. E. (1955). Non-steady Green's functions for an infinite strip of leaky aquifers. *Transactions of the American Geophysical Union*, *36*(1), 101. https://doi.org/10.1029/TR036i001p00101

Hemker, C. J. (1985). Transient well flow in leaky multiple-aquifer systems. *Journal of Hydrology*, *81*(1-2), 111–126. https://doi.org/10.1016/0022-1694(85)90170-2

Hemker, C. J., & Maas, C. (1994). Comment on "Multilayered leaky aquifer systems: 1. Pumping well solutions" by A. H.-D. Cheng, and O. K. Morohunfola. *Water Resources Research*, *30*(11), 3229–3230. https://doi.org/10.1029/94WR01802

Hornbach, M. J., DeShon, H. R., Ellsworth, W. L., Stump, B. W., Hayward, C., Frohlich, C., et al. (2015). Causal factors for seismicity near Azle, Texas. *Nature Communications*, *6*(1), 6728. https://doi.org/10.1038/ncomms7728

Hsieh, P., Bredehoeft, J., & Farr, J. (1987). Determination of aquifer permeability from earthtide analysis. *Water Resources Research*, *23*, 1824–1832.

Ingebritsen, S. E., & Manning, C. E. (2010). Permeability of the continental crust: Dynamic variations inferred from seismicity and metamorphism. *Geofluids*, *10*, 193–205. https://doi.org/10.1111/j.1468-8123.2010.00278.x

Ingebritsen, S. E., Sanford, W. E., & Neuzil, C. E. (2006). *Groundwater in geologic processes*, (2nd ed.). N. Y: Cambridge Univ. Press.

Johnson, K. S. (2008). Geologic history of Oklahoma, Oklahoma Geological Survey, Educational Publication 9.

Keranen, K. M., Savage, H. M., Abers, G. A., & Cochran, E. S. (2013). Potentially induced earthquakes in Oklahoma, USA: Links between wastewater injection and the 2011 M_w 5.7 earthquake sequence. *Geology*, *41*(6), 699–702. https://doi.org/10.1130/G34045.1

Keranen, K. M., Weingarten, M., Abers, G. A., Bekins, B. A., & Ge, S. (2014). Sharp increase in central Oklahoma seismicity since 2008 induced by massive wastewater injection. *Science*, *345*(6195), 448–451. https://doi.org/10.1126/science.1255802

Kroll, K. A., Cochran, E. S., & Murray, K. E. (2017). Poroelastic properties of the Arbuckle Group in Oklahoma derived from well fluid level response to the 3 September 2016 Mw5.8 Pawnee and 7 November 2016 M_w5.0 Cushing earthquakes. *Seismological Research Letters*, *88*(4), 963–970. https://doi.org/10.1785/0220160228

Lee, T.-C. (1999). *Applied mathematics in hydrogeology*. N. Y: Lewis publishers.

Liao, X., Wang, C.-Y., & Liu, C. P. (2015). Disruption of groundwater system by large earthquakes. *Geophysical Research Letters*, *42*, 9758–9763. https://doi.org/10.1002/2015GL066394

Li, X.-M., Zhao, B., Wang, Z., Xie, M., Song, J., Nghiem, L. D., et al. (2014). Water reclamation from shale gas drilling flow-back fluid using a novel forward osmosis–vacuum membrane distillation hybrid system. *Water Science and Technology*, *69*(5), 1036–1044. https://doi.org/10.2166/wst.2014.003

Liu, W., & Manga, M. (2009). Changes in permeability caused by dynamic stresses in fractured sandstone. *Geophysical Research Letters*, *36*, L20307. https://doi.org/10.1029/2009GL039852

Maas, C. (1987a). Groundwater flow to a well in a layered porous medium: 1. Steady flow. *Water Resources Research*, *23*(8), 1675–1681. https://doi.org/10.1029/WR023i008p01675

Maas, C. (1987b). Groundwater flow to a well in a layered porous medium: 2. Nonsteady multiple-aquifer flow. *Water Resources Research*, *23*(8), 1683–1688. https://doi.org/10.1029/WR023i008p01683

Manga, M., Beresnev, I., Brodsky, E. E., Elkhoury, J. E., Elsworth, D., Ingebritsen, S. E., et al. (2012). Changes in permeability by transient stresses: field observations, experiments and mechanisms. *Reviews of Geophysics*, *50*, RG2004. https://doi.org/10.1029/2011RG000382

Manga, M., Wang, C.-Y., & Shirzaei, M. (2016). Increased stream discharge after the 3 September 2016 M_w 5.8 Pawnee, Oklahoma earthquake. *Geophysical Research Letters*, *43*, 11,588–11,594. https://doi.org/10.1002/2016GL071268

McGarr, A., Bekins, B., Burkardt, N., Dewey, J., Earle, P., Ellsworth, W., et al. (2015). Coping with earthquakes induced by fluid injection. *Science*, *347*(6224), 830–831. https://doi.org/10.1126/science.aaa0494

McNamara, D. E., Benz, H. M., Herrmann, R. B., Bergman, E. A., Earle, P., Holland, A., et al. (2015). Earthquake hypo-centers and focal mechanisms in central Oklahoma reveal a complex system of reactivated subsurface strike-slip faulting. *Geophysical Research Letters*, *42*, 2742–2749. https://doi.org/10.1002/2014gl062730

Mohr, C. H., Manga, M., Wang, C.-Y., Kirchner, J. W., & Bronstert, A. (2015). Shaking water out of soil. *Geology*, *43*, 207–210.

Morgan, B. C., & Murray, K. E. (2015). Characterizing small-scale permeability of the Arbuckle Group, Oklahoma. Open File Report OF2–2015, 1–12. National Archives and Records Administration, 1989.

Rahi, K., & Halihan, T. (2009). *Estimating selected hydraulic parameters of the Arbuckle-Simpson aquifer from the analysis of naturally-induced stresses, Report, Oklahoma Water Resource Board.31. Wang, H.F., 2000, Theory of Linear Poroelasticity*, (p. 287). Princeton: Princeton University Press.

Roeloffs, A. (1996). Poroelastic techniques in the study of earthquake-related hydrology phenomenon. *Advances in Geophysics*, *37*(135–195), 1996.

Schoenball, M., & Ellsworth, W. L. (2017). A systematic assessment of the spatio-temporal evolution of fault activation through induced seismicity in Oklahoma and southern Kansas. *Journal of Geophysical Research: Solid Earth*, *122*, 10,189–10,206. https://doi.org/10.1002/2017JB014850

Sorenson, R. P. (2005). A dynamic model for the Permian Panhandle and Hugoton fields, wester Anadarko basin. *AAPG Bulletin*, *89*(7), 921–938. https://doi.org/10.1306/03010504045

Sun, A. Y., Lu, J., & Hovorka, S. (2015). A harmonic pulse testing method for leakage detection in deep subsurface storage formation. *Water Resources Research*, *51*, 4263–4281. https://doi.org/10.1002/2014WR016567

Tamura, Y., Sato, T., Ooe, M., & Ishiguro, M. (1991). A procedure for tidal analysis 73 17 with a Bayesian information criterion. *Geophysical Journal International*, *104*, 507–516.

U.S. Environmental Protection Agency (2016). *Hydraulic fracturing for oil and gas: Impacts from the hydraulic fracturing water cycle on drinking water resources in the United States*. Washington, DC: U.S. Environmental Protection Agency.

Veling, E. J. M., & Maas, C. (2009). Strategy for solving semi-analytically three-dimensional transient flow in a coupled N-layered aquifer system. *Journal of Engineering Mathematics*, *64*(2), 145–161. https://doi.org/10.1007/s/10665-008-9256-9

Vengosh, A., Jackson, R. B., Warner, N., Darrah, T., & Kondash, A. (2014). A critical review of the risks to water resources from unconventional shale gas development and hydraulic fracturing in the United States. *Environmental Science & Technology*, *48*(15), 8334–8348. https://doi.org/10.1021/es405118y

Vidic, R. D., Brantley, S. L., Vandenbossche, J. M., Yoxtheimer, D., & Abad, J. D. (2013). Impact of shale gas development on regional water quality. *Science*, *340*(6134). https://doi.org/10.1126/science.1235009

Walsh, F. R., & Zoback, M. D. (2015). Oklahoma's recent earthquakes and saltwater disposal. *Science Advances*, *1*(5), e1500195. https://doi.org/10.1126/sciadv.1500195

Wang, C.-Y., Liao, X., Wang, L.-P., Wang, C.-H., & Manga, M. (2016). Large earthquakes create vertical permeability by breaching aquitards. *Water Resources Research*, *52*, 5923–5937. https://doi.org/10.1002/2016WR018893

Wang, C.-Y., & Manga, M. (2015). New streams and springs after the 2014 Mw6.0 South Napa earthquake. *Nature Communications*, *6*, 7597. https://doi.org/10.1038/ncomms8597

Wang, C.-Y., Manga, M., Dreger, D., & Wong, A. (2004). Streamflow increase due to rupturing of hydrothermal reservoirs: Evidence from the 2003 San Simeon earthquake (2003), California, earthquake. *Geophysical Research Letters*, *31*, L10502. https://doi.org/10.1029/2004GL020124

Wang, C.-Y., Manga, M., Shirzaei, M., Weingarten, M., & Wang, L.-P. (2017). Induced seismicity in Oklahoma affects shallow groundwater. *Seismological Research Letters*, *88*(4), 956–962. https://doi.org/10.1785/0220170017

Wang, C.-Y., Manga, M., Wang, C. H., & Chen, C. H. (2012). Transient change in groundwater temperature after earthquakes. *Geology*, *40*(2), 119–122.

Wang, C.-Y., Wang, C. H., & Manga, M. (2004). Coseismic release of water from mountains: Evidence from the 1999 (Mw = 7.5) Chi-Chi, Taiwan, earthquake. *Geology*, *32*, 769–772.

Wang, C.-Y., Wang, L.-P., Manga, M., Wang, C.-H., & Chen, C.-H. (2013). Basin-scale transport of heat and fluid induced by earthquakes. *Geophysical Research Letters*, *40*, 3893–3897. https://doi.org/10.1002/grl.50738

Wang, H. F. (2000). *Theory of linear poroelasticity with applications to geomechanics and hydrogeology*. Princeton, New Jersey: Princeton University Press.

Weingarten, M., Ge, S., Godt, J. W., Bekins, B. A., & Rubinstein, J. L. (2015). High-rate injection is associated with the increase in U.S. mid-continent seismicity. *Science*, *348*(6241), 1336–1340. https://doi.org/10.1126/science.aab1345

Xue, L., Brodsky, E. E., Erskine, J., Fulton, P. M., & Carter, R. (2016). A permeability and compliance contrast measured hydrogeologically on the San Andreas Fault. *Geochemistry, Geophysics, Geosystems*, *17*, 858–871. https://doi.org/10.1002/2015GC006167

Yeck, W. L., Hayes, G. P., McNamara, D. E., Rubinstein, J. L., Barn- hart, W. D., Earle, P. S., & Benz, H. M. (2016). Oklahoma experiences largest earthquake during ongoing regional wastewater injection hazard mitigation efforts. *Geophysical Research Letters*, *44*, 711–717. https://doi.org/10.1002/2016GL071685

Yeck, W. L., Weingarten, M., Benz, H. M., McNamara, D. E., Berg- man, E. A., Herrmann, R. B., et al. (2016). Far-field pressurization likely caused one of the largest injection induced earthquakes by reactivating a large preexisting basement fault structure. *Geophysical Research Letters*, *43*, 10,198–10,207. https://doi.org/10.1002/2016GL070861

Zhang, Y., Fu, L. Y., Huang, F. Q., & Chen, X. Z. (2015). Co-seismicwaterlevel changes in a well induced by teleseismic waves from three lar- geearthquakes. Tectonophysics, 6517–652, 232–241.

Zhang, Y., Person, M., Rupp, J., Ellett, K., Celia, M. A., Gable, C. W., et al. (2013). Hydrogeologic controls on induced seismicity in crystalline basement rocks due to fluid injection into basal reservoirs. *Groundwater*, *51*(4), 525–538. https://doi.org/10.1111/gwat.12071